CORONAVIRUS

ACE2-binding exposes the SARS-CoV-2 fusion peptide to broadly neutralizing coronavirus antibodies

Jun Siong Low[1,2]*†, Josipa Jerak[1,2]†, M. Alejandra Tortorici[3]†, Matthew McCallum[3]‡, Dora Pinto[4]‡, Antonino Cassotta[1], Mathilde Foglierini[1], Federico Mele[1], Rana Abdelnabi[5], Birgit Weynand[6], Julia Noack[7], Martin Montiel-Ruiz[7], Siro Bianchi[4], Fabio Benigni[4], Nicole Sprugasci[4], Anshu Joshi[3], John E. Bowen[3], Cameron Stewart[3], Megi Rexhepaj[3], Alexandra C. Walls[3,8], David Jarrossay[1], Diego Morone[1], Philipp Paparoditis[1], Christian Garzoni[9], Paolo Ferrari[10,11,12], Alessandro Ceschi[10,13,14,15], Johan Neyts[5,16], Lisa A. Purcell[7], Gyorgy Snell[7], Davide Corti[4], Antonio Lanzavecchia[4,17]§, David Veesler[3,8]*§, Federica Sallusto[1,2]*§

The coronavirus spike glycoprotein attaches to host receptors and mediates viral fusion. Using a broad screening approach, we isolated seven monoclonal antibodies (mAbs) that bind to all human-infecting coronavirus spike proteins from severe acute respiratory syndrome coronavirus 2 (SARS-CoV-2) immune donors. These mAbs recognize the fusion peptide and acquire affinity and breadth through somatic mutations. Despite targeting a conserved motif, only some mAbs show broad neutralizing activity in vitro against alpha- and betacoronaviruses, including animal coronaviruses WIV-1 and PDF-2180. Two selected mAbs also neutralize Omicron BA.1 and BA.2 authentic viruses and reduce viral burden and pathology in vivo. Structural and functional analyses showed that the fusion peptide–specific mAbs bound with different modalities to a cryptic epitope hidden in prefusion stabilized spike, which became exposed upon binding of angiotensin-converting enzyme 2 (ACE2) or ACE2-mimicking mAbs.

The *Orthocoronavirinae* subfamily of coronaviruses comprises four genera: *Alphacoronavirus*, *Betacoronavirus*, *Gammacoronavirus*, and *Deltacoronavirus*. Alphacoronaviruses NL63 and 229E and betacoronaviruses OC43, HKU1, severe acute respiratory syndrome coronavirus 2 (SARS-CoV-2), SARS-CoV, and Middle East respiratory syndrome (MERS)-CoV account for almost all human coronavirus (hCoV) infections, with sporadic infections attributed to canine alphacoronavirus CCoV-HuPn-2018 and porcine deltacoronavirus (PDCoV) (*1*–*3*). The spike (S) glycoprotein, which binds to various host receptors for viral entry (table S1), is composed of the S_1 and S_2 subunits, is highly divergent, with only ~30% sequence identity between alpha- and betacoronaviruses, and is the main target of neutralizing antibodies (*4*–*7*). Previous studies have described neutralizing monoclonal antibodies (mAbs) that cross-react among sarbecoviruses by targeting the receptor-binding domain (RBD) in the S_1 subunit (*8*–*14*) or more broadly across betacoronaviruses by targeting the stem helix in the S_2 subunit (*15*–*20*). However, mAbs neutralizing both alpha- and betacoronaviruses have not been reported. Broadly neutralizing mAbs, as exemplified by those targeting influenza viruses or HIV-1 (*21*–*26*), can potentially be used for prophylaxis or therapy and to guide the design of vaccines eliciting broadly protective immunity (*27*, *28*).

Isolation of broadly reactive coronavirus mAbs from convalescent and vaccinated individuals

To search for antibodies that cross-react with human-infecting alpha- and betacoronaviruses, we stimulated, under limiting conditions, total peripheral blood mononuclear cells (PBMCs) from SARS-CoV-2 immune donors in the presence of the TLR7/8 agonist R848 and interleukin-2 (IL-2), which selectively induce the proliferation and differentiation of memory B cells (*29*). On day 12, the specificities of immunoglobulin G (IgG) secreted in the culture supernatants were tested by enzyme-linked immunosorbent assay (ELISA) against a panel of recombinant S proteins from alpha and beta hCoVs (Fig. 1, A to C). The number of SARS-CoV-2 S IgG–positive cultures was generally higher in COVID-19 convalescent patients and in SARS-CoV-2 vaccinees with prior infection (preimmune) compared with vaccinees without prior infection (naïve). Most SARS-CoV-2 S IgG–positive cultures were either monospecific or cross-reactive with the closely related SARS-CoV S, whereas a small fraction was also reactive with OC43 and HKU1 S (Fig. 1, A to D), consistent with previous serological analyses (*17*, *30*, *31*). Six cultures (of >4000) from five individuals (of 43) cross-reacted with all alpha and beta hCoV S proteins tested (Fig. 1, A to D), suggesting that memory B cells producing broadly reactive coronavirus antibodies might exist at very low frequency.

To isolate broadly reactive coronavirus mAbs, we combined the screening of polyclonally activated memory B cells with the sorting and cloning of antibody-secreting cells to retrieve paired heavy- and light-chain sequences (fig. S1). Using this approach, we isolated 16 SARS-CoV-2 S-specific mAbs that cross-reacted with various hCoV S proteins (Fig. 1E and fig. S2A). Six mAbs (group 1) cross-reacted with the betacoronaviruses SARS-CoV, SARS-CoV-2, OC43, and HKU1 S proteins, with median effective concentration (EC_{50}) values ranging from 45 to 3000 ng/ml. Three mAbs (group 2) cross-reacted with high affinity to all beta hCoV S proteins, with EC_{50} values ranging from 18 to 40 ng/ml (Fig. 1E). These mAbs were found to target the stem helix region and have been described in a separate study (*15*). The remaining seven mAbs (group 3) exhibited the broadest cross-reactivity to both alpha and beta hCoV S proteins, with EC_{50} values ranging from 29 to 800 ng/ml (Fig. 1E). These broadly reactive mAbs, which are the focus of the present study, were isolated from convalescent or vaccinated individuals, used different V genes (except for C13B8 and C13A7, which are clonally related), and displayed a high load of somatic mutations (7 to 14% in VH, 2 to 8% in VL at the nucleotide level; table S2). These results illustrate the utility of a simple high-throughput method based on multiple parallel screening steps of memory B cells to isolate broadly reactive coronavirus mAbs.

Broadly reactive mAbs bind to the fusion peptide and acquire affinity and breadth through somatic mutations

Using SARS-CoV-2 S_1, RBD, and S_2 protein domains, as well as 15-mer linear peptides covering the entire S sequence, the specificities of all seven group 3 mAbs were mapped to the K811PSKRSFIEDLLFNK825 sequence in the SARS-CoV-2 S_2 subunit (Fig. 2A). This sequence spans the S_2' cleavage site (R815) and the fusion peptide N-terminal region, which is essential for membrane fusion (*32*) and is highly conserved among all genera of the *Orthocoronavirinae* subfamily, including deltacoronavirus PDCoV and gammacoronavirus IBV, as well as all

[1]Institute for Research in Biomedicine, Università della Svizzera Italiana, 6500 Bellinzona, Switzerland. [2]Institute of Microbiology, ETH Zürich, 8093 Zurich, Switzerland. [3]Department of Biochemistry, University of Washington, Seattle, WA 98195, USA. [4]Humabs BioMed SA (subsidiary of Vir Biotechnology), 6500 Bellinzona, Switzerland. [5]KU Leuven Department of Microbiology, Immunology and Transplantation, Rega Institute for Medical Research, Laboratory of Virology and Chemotherapy, B-3000 Leuven, Belgium. [6]KU Leuven Department of Imaging and Pathology, Translational Cell and Tissue Research, B-3000 Leuven, Belgium. [7]Vir Biotechnology, San Francisco, CA 94158, USA. [8]Howard Hughes Medical Institute, Seattle, WA 98195, USA. [9]Clinic of Internal Medicine and Infectious Diseases, Clinica Luganese Moncucco, 6900 Lugano, Switzerland. [10]Faculty of Biomedical Sciences, Università della Svizzera Italiana, 6900 Lugano, Switzerland. [11]Department of Internal Medicine, Ente Ospedaliero Cantonale, 6500 Bellinzona, Switzerland. [12]Prince of Wales Hospital Clinical School, University of New South Wales, Sydney, New South Wales 2052, Australia. [13]Division of Clinical Pharmacology and Toxicology, Institute of Pharmacological Sciences of Southern Switzerland, Ente Ospedaliero Cantonale, 6900 Lugano, Switzerland. [14]Clinical Trial Unit, Ente Ospedaliero Cantonale, 6500 Bellinzona, Switzerland. [15]Department of Clinical Pharmacology and Toxicology, University Hospital Zurich, 8091 Zurich, Switzerland. [16]Global Virus Network, Baltimore, MD 21201, USA. [17]National Institute of Molecular Genetics, 20122 Milano, Italy.
***Corresponding author. Email: sallustf@ethz.ch (F.S.); junsiong.low@biol.ethz.ch (J.S.L.); dveesler@uw.edu (D.V.)**
†These authors contributed equally to this work.
‡These authors contributed equally to this work.
§These authors contributed equally to this work.

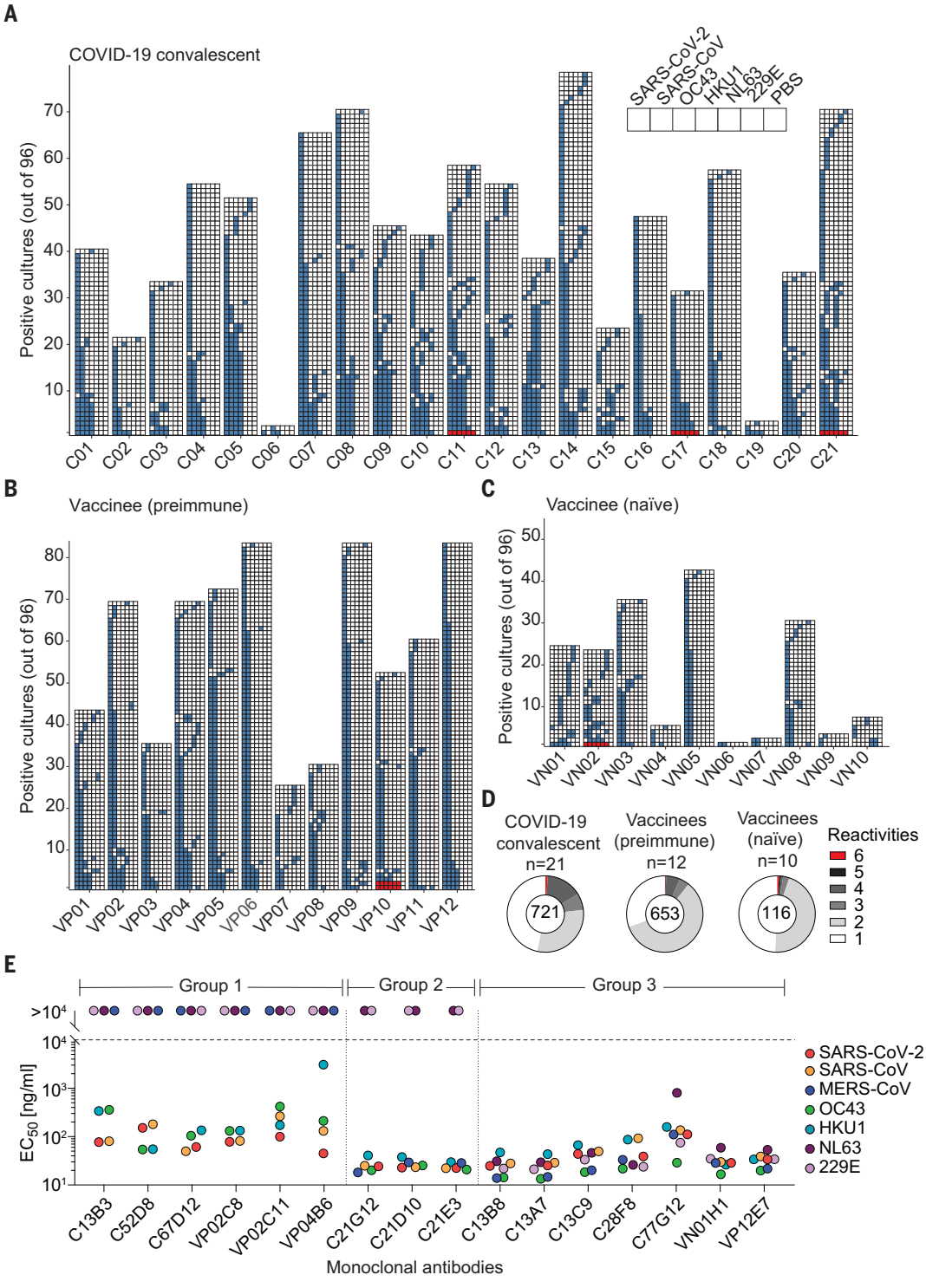

Fig. 1. Rare broadly reactive memory B cells are elicited upon natural infection or vaccination. (**A** to **D**) Total PBMCs from COVID-19 convalescents (C) (A), vaccinees with prior infection (preimmune) (VP) (B), and vaccinees without prior infection (naïve) (VN) (C) (table S5) were plated in replicate 96 wells (10^4 cells/well) and stimulated with the TLR7/8 agonist R848 (2.5 μg/ml) in the presence of IL-2 (1000 U/ml). Twelve days later, the supernatant of each culture was screened, in parallel, for the specificities of the secreted IgG antibodies to commercially available hCoV S proteins from SARS-CoV-2, SARS-CoV, OC43, HKU1, NL63, and 229E by ELISA. The skyline plot provides a detailed view of the specificities of each culture well (represented in rows) to the respective antigens (in subcolumn) from each donor (in column). The order of the antigens is indicated in the legend and uncoated plates (phosphate-buffered saline, PBS) were used as control. If the optical density at 405 nm (OD_{405}) value exceeded the cutoff value determined by average OD_{405} of PBS wells ± 4*standard deviation, the culture was considered reactive to the antigen and is indicated here with colored cells. Only cultures exhibiting reactivity to at least one antigen are shown. Red cells highlight the six cultures exhibiting reactivity to all alpha and beta hCoV S proteins tested. (D) Cross-reactivity patterns of SARS-CoV-2 S–positive cultures from (A) to (C) are shown as pie charts. The total number of SARS-CoV-2 S–positive cultures from each cohort is indicated at the center of the pie. (**E**) Using a two-step screening strategy as depicted in fig. S1, 16 mAbs that cross-reacted with multiple hCoV S proteins were isolated from 10 donors. Shown are EC_{50} values to the respective commercially available hCoV S proteins measured by ELISA. mAbs are grouped on the basis of reactivity patterns. Shown is one representative experiment out of at least two performed. Group 2 mAbs C21G12, C21D10, and C21E3 were described in a separate study (*15*) (designated P34G12, P34D10, and P34E3, respectively).

SARS-CoV-2 variants sequenced to date (fig. S3, A and B). Most of the seven group 3 mAbs bound more tightly to the prefusion SARS-CoV-2 S trimer without stabilizing proline substitution in the fusion peptide (PentaPro) relative to HexaPro (F817P) (*33*), and all of them bound with greater avidity to prefusion SARS-CoV-2 S_2 compared with postfusion S_2 (Fig. 2A and fig. S2D).

To explore the ontogeny of the isolated fusion peptide–specific mAbs, we compared the binding properties of mature mAbs to their unmutated common ancestors (UCAs) (Fig. 2B and fig. S2B). The UCAs of C13B8, C13A7 (the two clonally related mAbs), and VN01H1 exhibited broad reactivity with hCoV S proteins but had lower affinity than their mature counterparts. By contrast, the C13C9 UCA bound only to the beta hCoVs OC43 and MERS-CoV S,

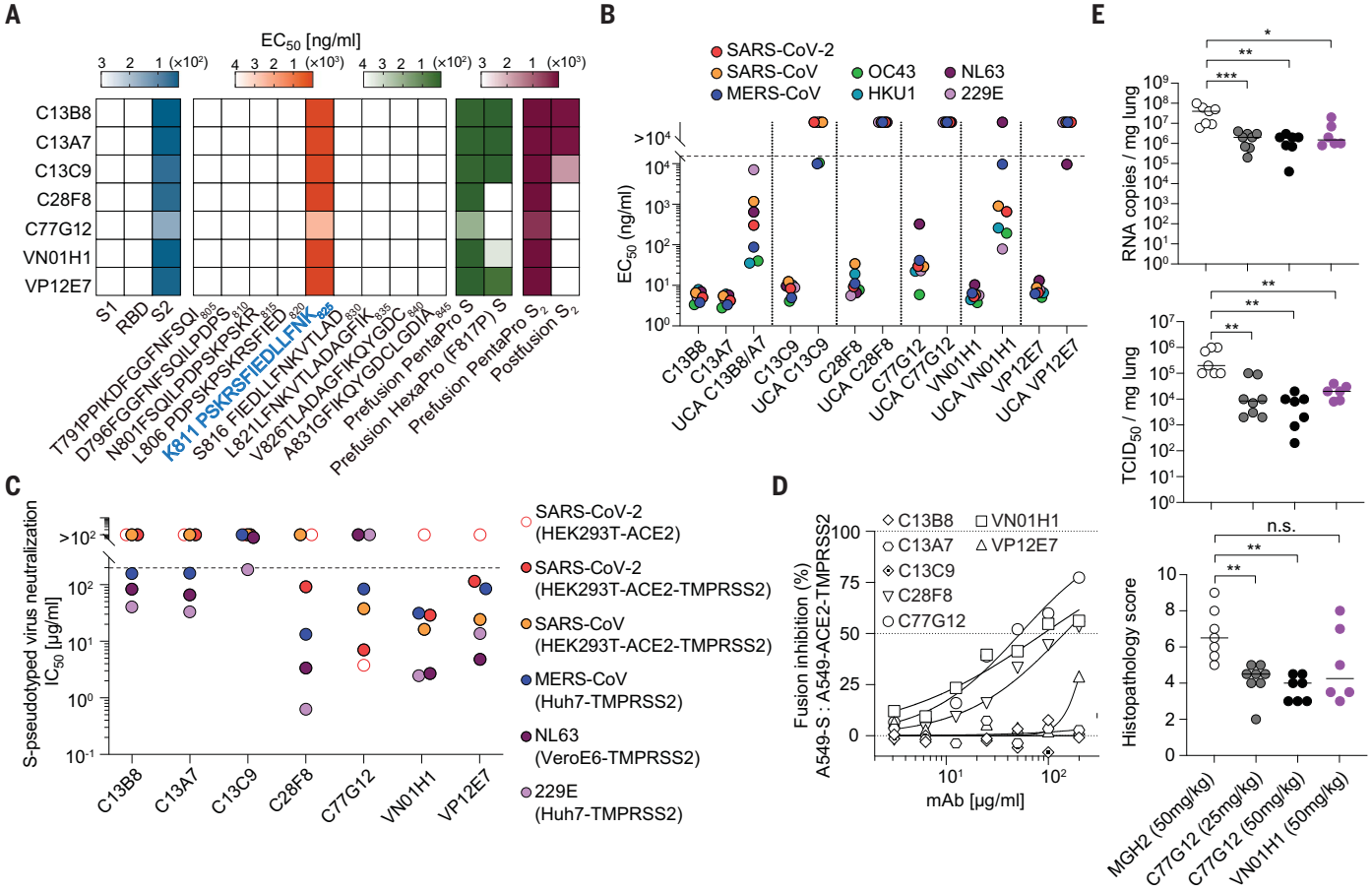

Fig. 2. Broadly reactive fusion peptide-specific mAbs acquire affinity and breadth through somatic mutations. (**A**) Binding profiles of the seven group small Group 3 mAbs. Epitope mapping was performed using commercially available SARS-CoV-2 protein domains (S_1, RBD, and S_2), 15-mer overlapping synthetic peptides with the indicated sequences, prefusion HexaPro (F817P) S, prefusion PentaPro (F817) S, prefusion PentaPro (F817) S_2, and postfusion S_2 coated onto plastic and assessed by ELISA (log_{10} EC_{50} shown). The mAbs all recognized the fusion peptide sequence highlighted in blue. (**B**) Binding evaluation of group 3 mAbs and their respective germline reverted UCAs to different hCoV S proteins. C13B8 and C13A7 are sister clones and thus share a single UCA. One representative experiment of at least two is shown. (**C**) Half-maximum inhibitory concentrations (IC_{50}s) of group 3 mAbs against SARS-CoV-2, SARS-CoV, MERS-CoV, NL63, and 229E S-pseudotyped viruses in the indicated target cell lines. For each hCoV pseudotyped assay, all mAbs were compared in parallel. One representative experiment of at least two is shown. (**D**) Group 3 mAbs were assessed for their ability to inhibit the fusion of SARS-CoV-2 S–expressing (A549-S) and ACE2-TMPRSS2–expressing (A549-ACE2-TMPRSS2) A549 cells. Inhibition of fusion values are normalized to the percentage of fusion without mAb (100%) and to that of fusion of non-transfected cells (0%). One representative experiment of two is shown. (**E**) The prophylactic efficacy of VN01H1 (50 mg/kg), C77G12 (25 and 50 mg/kg), and the negative control malaria-specific mAb MGH2 (50 mg/kg) were tested in hamsters challenged with the SARS-CoV-2 P.1 (Gamma) variant of concern. Viral RNA loads (top), replicating virus titers (middle), and histopathological scores (bottom) are shown. $P > 0.05$ (non-significant, n.s.), $^{*}P \le 0.05$, $^{**}P \le 0.01$, $^{***}P \le 0.001$, Mann-Whitney test corrected using Bonferroni multiple comparisons.

whereas the VP12E7 UCA bound only to the alpha hCoV NL63 S, with low affinity in both cases. Finally, the UCAs of C28F8 and C77G12 did not bind to any hCoV S proteins tested. Given the lack of a common V gene usage, these findings suggest that broadly reactive fusion peptide–specific mAbs can mature through multiple pathways and acquire high affinity and cross-reactivity through somatic mutations, possibly because of priming by endemic coronavirus infection followed by SARS-CoV-2 boosting upon infection or vaccination.

Considering the high conservation of the fusion peptide region, we next assessed whether broad reactivity is a property shared by most fusion peptide–specific mAbs. IgGs secreted upon polyclonal activation of memory B cells from 71 convalescent individuals were screened for binding to a pool of alpha and beta hCoV fusion peptides, as well as to SARS-CoV-2 S protein. Cultures producing fusion peptide–specific mAbs were detected at low frequency and only in 19 individuals (fig. S4A). Although nearly all fusion peptide–reactive mAbs bound to SARS-CoV-2 S, only nine of 30 were broadly reactive, and the remaining mAbs showed different degrees of cross-reactivity (fig. S4B). Thus, although the coronavirus S fusion peptide is conserved (*34*–*39*), broad reactivity is the property of a minority of fusion peptide–specific mAbs, consistent with the observation that only three of the seven group 3 mAbs cross-reacted with the PDCoV and IBV fusion peptides (fig. S3C).

Fusion peptide-specific mAbs have heterogeneous neutralizing activities and can reduce viral burden in vivo

We next tested the neutralizing activity of all seven group 3 mAbs against pseudotyped viruses carrying S proteins of alpha- and beta-coronaviruses. Despite binding to the same motif, these mAbs exhibited distinct neutralizing potencies. Most notably, VN01H1 and VP12E7 neutralized all hCoV S–pseudotyped viruses tested (SARS-CoV-2, SARS-CoV, MERS-CoV, NL63, and 229E), as well as bat sarbecovirus WIV-1 and merbecovirus PDF-2180 (*40*)

S–pseudotyped viruses (Fig. 2C and fig. S5, A to C). C77G12 neutralized all betacoronavirus S pseudotype viruses tested with the highest relative potency for SARS-CoV-2 (Fig. 2C and fig. S5, A to C). The SARS-CoV-2–neutralizing activity of VN01H1 and C77G12 was reduced by the addition of soluble fusion peptide (fig. S5D). Furthermore, VN01H1, C77G12, and C28F8 also inhibited SARS-CoV-2 S–mediated cell-cell fusion (Fig. 2D), suggesting that fusion peptide–specific mAbs could prevent S proteolytic activation or fusogenic rearrangements, thereby inhibiting membrane fusion and viral entry.

We next assessed the protective efficacy of the VN01H1 and C77G12 mAbs in vivo. In the Syrian hamster model of SARS-CoV-2 P.1 (Gamma) infection, prophylactic administration of either mAb at high doses reduced viral RNA copies and lung titers and ameliorated lung pathology at statistically significant levels (Fig. 2E). These findings demonstrate that fusion peptide–specific mAbs can reduce viral burden in vivo, albeit with moderate potency.

Structural basis for fusion peptide recognition

To gain insight into the epitope recognized by fusion peptide–specific broadly reactive coronavirus mAbs, we performed substitution scan and structural analysis on the six clonally unrelated mAbs. All mAbs bound to a core motif comprising I818EDLLFNK825 (fig. S6A), with C28F8, C77G12, VN01H1, and VP12E7 having a three–amino acid expanded footprint spanning the N-terminal R815SF817 residues, which includes the S_2' cleavage site at position R815.

We determined the crystal structures of five Fabs (C13B8, C13C9, C77G12, VN01H1, and VP12E7) in complex with the K811PSKRSFIEDLLFNK825 fusion peptide at 2.1 Å, 2.1 Å, 1.7 Å, 1.86 Å, and 2.5 Å, resolution, respectively (Fig. 3; fig. S6, B to D; and table S3). All five Fabs bind to overlapping epitopes in the fusion peptide through interactions involving the heavy- and light-chains. The strict conservation and the conservative substitution of key residues involved in mAb recognition (R815, S816, I818, E819, D820, L821, L822, F823, N824, and K825) across the *Orthocoronavirinae* subfamily explains the broad cross-reactivity of these fusion peptide–specific mAbs (figs. S3 and S6 and table S4). The overall architecture of the fusion peptide in the C13C9-bound complex structure is most similar to that observed in the prefusion S trimer (PDB 6VXX) (*4*) (Fig. 3C and fig. S6B). In the two structures determined in complex with VN01H1 or VP12E7, the SARS-CoV-2 S fusion peptide adopts a similar conformation, which is distinct from the conformation observed in prefusion SARS-CoV-2 S trimeric structures (*4*) (Fig. 3, B and C, and fig. S6C). Specifically, residues 813SKR815 refold from an extended conformation in prefusion S to an α-helical conformation in the two Fab-bound peptide structures, thereby

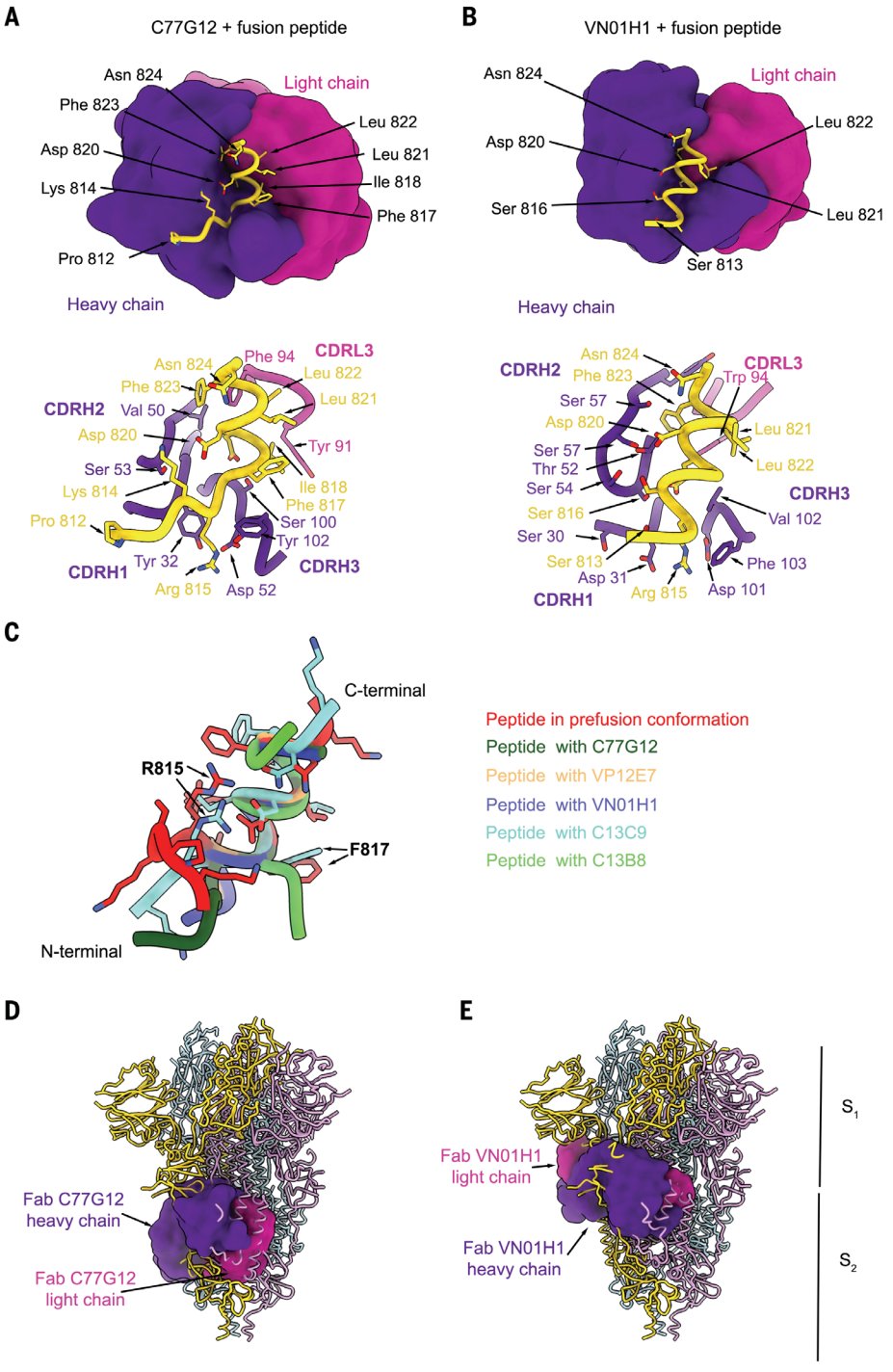

Fig. 3. Fusion peptide-specific antibodies target a cryptic epitope. (**A** and **B**) (Top) Surface representation of the crystal structures of the C77G12 (A) and VN01H1 (B) Fabs in complex with SARS-CoV-2 fusion peptide epitope. (Bottom) Ribbon representation of the corresponding structures highlighting the interactions of Fab heavy- and light-chain complementarity-determining regions with the fusion peptide (selected regions are shown for clarity). (**C**) Ribbon representation of the fusion peptides in the Fab-bound complexes superimposed with the fusion peptide in prefusion SARS-CoV-2 S (PDB 6VXX). (**D** and **E**) Superimposition of the C77G12-bound (D) or VN01H1-bound (E) fusion peptide structures to prefusion SARS-CoV-2 S uncovering the cryptic nature of the epitope. The Fabs are shown as surfaces, and S is rendered as ribbons. Each SARS-CoV-2 S protomer is colored distinctly (light blue, pink, and gold), and Fab heavy and light chains are colored purple and magenta, respectively.

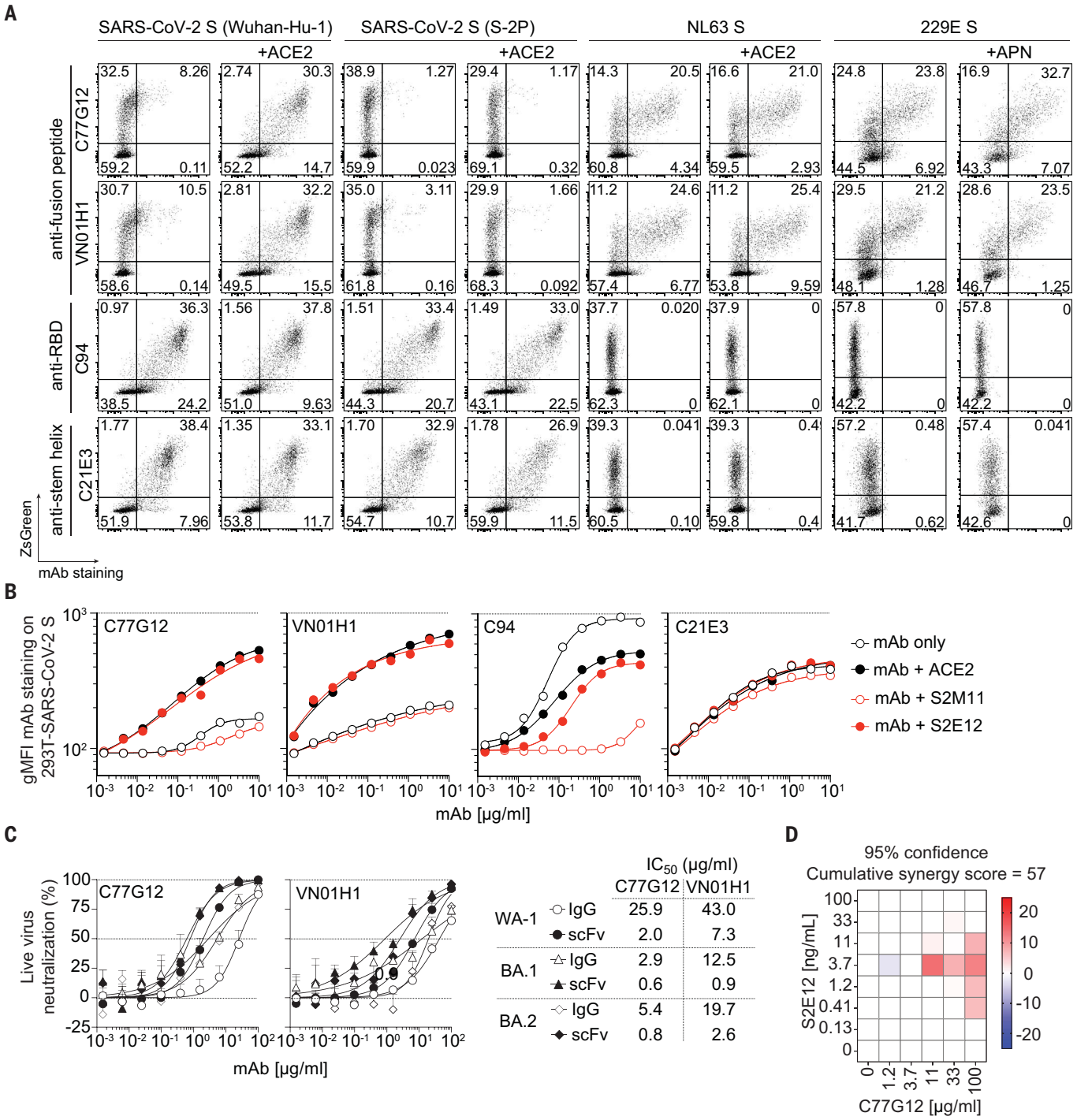

Fig. 4. The SARS-CoV-2 fusion peptide is unmasked after ACE2 receptor engagement. (**A**) Binding of fusion peptide–specific mAbs VN01H1 and C77G12 (8 μg/ml), as well as RBD-specific C94 and stem helix–specific C21E3 mAbs (8 μg/ml) on HEK293T cells transiently cotransfected with plasmid encoding ZsGreen and plasmids encoding full-length SARS-CoV-2 S Wuhan-Hu-1 (GenBank: NC_045512), SARS-CoV-2 S-2P (K986P, V987P), NL63 S (GenBank: APF29071.1), or 229E S (GenBank: APT69883.1) in the presence or absence of respective recombinant receptors ACE2 or APN, as measured by flow cytometry. (**B**) Titrating doses of fluorescently labeled mAbs were coincubated with HEK293T cells expressing full-length SARS-CoV-2 S for 2 hours at room temperature in the presence or absence of recombinant ACE2-mFc (27 μg/ml), ACE2-mimicking mAb S2E12 (20 μg/ml), or S2M11 (20 μg/ml). The latter mAb locks the S trimer in a closed conformation. The line in the scatter plot is a reference for the maximum geometric mean fluorescence intensity (gMFI) of staining with control anti-RBD C94 mAb. One representative experiment of two is shown. (**C**) VN01H1 and C77G12 in full-length IgG or scFv formats were tested for their neutralization of authentic SARS-CoV-2 Washington-1 and Omicron BA.1 and BA.2 variants. IC_{50} values are displayed as a table. (**D**) Synergy experiment performed against SARS-CoV-2 (Wuhan-Hu-1) S-pseudotyped virus (0.1 MOI) on VeroE6-TMPRSS2 at the indicated concentrations of S2E12 and C77G12 mAbs alone or in combination in a checkerboard manner. Analysis of mAb synergy was performed using MacSynergy II (*70*). Synergy plots adjusted with Bonferroni correction at 95% confidence were used for reporting. A synergy score between 50 and 100 was defined as moderate.

extending the α-helix found at the N-terminal region of the fusion peptide. In the C77G12-bound complex structure, the fusion peptide residues P812 to R815 adopt an extended conformation, distinct from prefusion S (Fig. 3, A and C), whereas these residues are disordered in the C13B8-bound structure (Fig. 3C and fig. S6D). The conserved residue R815, which is the S_2' site of proteolytic processing upon receptor binding for membrane fusion activation, is engaged in electrostatic interactions with the C13C9, VN01H1, VP12E7, and C77G12 Fabs and is therefore buried at the interface with their paratopes (table S4). Because preincubation of a soluble, native-like SARS-CoV-2 S ectodomain trimer with fusion peptide–specific mAbs did not prevent S2X58-induced triggering of fusogenic conformational changes (*41*, *42*) (fig. S7), these mAbs likely inhibit TMPRSS2 cleavage of the S_2' site (through steric hindrance) and in turn activation of membrane fusion. Although residue F817 is not part of the epitope (table S4), the F817P substitution present in the HexaPro construct likely prevents the adoption of the extended α-helical conformation observed in the structures bound to VN01H1 or VP12E7 (because of restricted backbone torsion angles), resulting in dampened binding in ELISA (Fig. 2A and fig. S2D).

Superimposition of the Fab-fusion peptide complexes with available prefusion S structure (PDB 6VXX) (*4*, *5*) revealed that the targeted epitope is buried toward the core of the S trimer and is therefore inaccessible (Fig. 3, D and E, and fig. S6, B to D), likely explaining the lack of detectable complexes of Fabs with prefusion S trimers during single-particle electron microscopy analysis. Taken together, these findings suggest that the epitope recognized by fusion peptide–specific mAbs is cryptic and may become accessible only transiently (*43*).

The fusion peptide is unmasked by ACE2 binding

To investigate the neutralization mechanism of fusion peptide–specific mAbs, we transfected human embryonic kidney 293T (HEK293T) cells to express coronavirus S proteins on their cell surface. All fusion peptide–specific mAbs showed only marginal binding to SARS-CoV-2 S–expressing HEK293T cells compared with control mAbs targeting the RBD (C94) (fig. S2C) or the stem helix (C21E3) (Fig. 4A and fig. S8A). However, the addition of soluble ACE2 enhanced binding of all fusion peptide-specific mAbs to SARS-CoV-2 S to levels comparable to that of the C94 and C21E3 control mAbs, suggesting that receptor engagement induces a conformational change that exposes the cryptic fusion peptide epitope (Fig. 4, A and B, and fig. S8A). This ACE2-dependent enhancement of binding was also observed with SARS-CoV-2 S harboring a deletion in the polybasic S_1/S_2 cleavage site (ΔPRRA) (*44*, *45*) (fig. S8A), suggesting that these mAbs can bind before S_1 shedding or S fusogenic refolding to postfusion state, consistent with the preferential binding to prefusion S_2 relative to postfusion S_2 (fig. S2A). However, the 2P (K986P, V987P) prefusion-stabilizing mutations (*4*, *5*) that lie outside of the epitope (Fig. 4A and fig. S8A) inhibited ACE2-mediated enhancement of mAb binding, implying an impediment of receptor-induced allosteric conformational changes, consistent with recent findings (*46*). Enhanced binding of fusion peptide–specific mAbs was also observed with SARS-CoV S– and MERS-CoV S–expressing HEK293T cells in the presence of their respective receptors ACE2 (*47*) and DPP4 (*48*). By contrast, fusion peptide-specific mAbs bound efficiently to HEK293T cells displaying the alphacoronaviruses NL63 and 229E S independently of receptor engagement by ACE2 (*49*) or APN (*50*), respectively (Fig. 4A and fig. S8A). We observed that VN01H1 and C77G12 neutralized authentic SARS-CoV-2 Omicron BA.1 and BA.2 more potently than Washington-1, likely because of increased accessibility of the fusion peptide in Omicron S (*46*). Furthermore, the neutralization potencies of VN01H1 and C77G12 could be further improved by engineering mAbs with smaller formats (such as scFv), suggesting possible limited accessibility of the fusion peptide region (Fig. 4C).

It was previously shown that certain mAbs can mimic ACE2 binding and trigger fusogenic activity (*51*, *52*). Indeed, the addition of S2E12, an ACE2-mimicking mAb, but not S2M11, a mAb that locks SARS-CoV-2 S trimer in the closed state (*51*), enhanced binding of the fusion peptide-specific mAbs (Fig. 4B). Consistent with this finding, we observed a synergy in pseudovirus neutralization when C77G12 was used in combination with S2E12 (Fig. 4D), suggesting that fusion peptide-specific mAbs may be more effective in the context of a polyclonal antibody response against the RBD. Collectively, these results indicate that the fusion peptide epitope only becomes accessible upon receptor-induced S conformational changes in sarbecovirus SARS-CoV-2, SARS-CoV, and merbecovirus MERS-CoV, whereas it is more readily accessible in the alphacoronaviruses NL63 and 229E, possibly because of molecular breathing to different extents in these S trimers.

Discussion

Using a high-throughput screening of memory B cells from immune donors with a panel of S proteins, we identified a new class of mAbs that target the fusion peptide region. These mAbs have different binding modalities, some of which exhibit unprecedented cross-reactivity to the fusion peptide of all four coronavirus genera. The findings that the UCAs of some of these mAbs bind preferentially to common cold coronaviruses and that the mAbs acquire affinity and breadth through somatic mutations suggest that their elicitation may require multiple rounds of selection, possibly by heterologous coronavirus infections. A complex developmental pathway has been reported for HIV-1–neutralizing mAbs and may be a general requirement for mAbs that recognize highly conserved epitopes (*53*, *54*).

Previous studies have identified serum antibodies binding to the fusion peptide of SARS-CoV-2 and showed, through depletion or peptide inhibition experiments, that such antibodies can contribute to the serum-neutralizing activity in a polyclonal setting (*34*–*38*). We show here that some fusion peptide–specific mAbs have direct neutralizing activity in vitro against alpha- and betacoronaviruses and can ameliorate pathology and viral burden in vivo at high doses. Although the neutralizing activity of these mAbs is low when used alone, it is possible that in the context of a polyclonal response, they may synergize with other antibodies that favor the exposure of the fusion peptide region, as shown here with S2E12.

The biochemical events associated with S_2' proteolytic processing for SARS-CoV, SARS-CoV-2, and MERS-CoV that are critical for unmasking the fusion peptide region have been described previously (*55*–*59*). The mAbs isolated in this study provide tools to characterize allosteric conformational changes in S triggered by receptor binding or by receptor-mimicking mAbs (*51*, *52*), a process that has thus far eluded structural definition. These events lead to exposure of the fusion peptide region for proteolytic cleavage by TMPRSS2 or endosomal cathepsins preceding membrane fusion (*32*). The finding that this region is readily accessible in alphacoronaviruses is consistent with the higher neutralizing activity of some fusion peptide–specific mAbs against NL63 and 229E and proposes that conformational changes might occur spontaneously as a consequence of molecular breathing.

Broadly neutralizing mAbs recognizing the fusion peptide region of influenza virus hemagglutinin and HIV-1 gp120 have guided the design of universal vaccine candidates against these highly variable pathogens (*60*–*66*). Similarly, the conservation of the fusion peptide region across the *Orthocoronavirinae* subfamily provides a rationale to develop a vaccine capable of inducing fusion peptide–specific responses that may be less prone to viral escape because of the potential fitness loss of escape mutants (*67*, *68*). The finding that prefusion stabilizing 2P mutations (*4*, *5*) abolish receptor-induced exposure of the fusion peptide suggests that current mRNA vaccines may be suboptimal in inducing antibody responses against this region. The broadly neutralizing coronavirus mAbs described in this study may be used as probes to design immunogens that can better

unmask the fusion peptide region and elicit broadly protective antibody responses. Notably, the fusion peptide region was also found to stimulate broadly reactive CD4 T cells (*69*), providing a cue for intramolecular help in the generation of such antibodies. In conclusion, our study identifies neutralizing mAbs with unprecedented breadth and sheds light on a receptor-triggered conformational change that limits the immunogenicity of this conserved region, with potential impacts on universal coronavirus vaccine design.

REFERENCES AND NOTES

1. A. N. Vlasova *et al*., *Clin. Infect. Dis.* **74**, 446–454 (2022).
2. J. A. Lednicky *et al*., *Nature* **600**, 133–137 (2021).
3. M. A. Tortorici *et al*., *Cell* **185**, 2279–2291.e17 (2022).
4. A. C. Walls *et al*., *Cell* **181**, 281–292.e6 (2020).
5. D. Wrapp *et al*., *Science* **367**, 1260–1263 (2020).
6. L. Piccoli *et al*., *Cell* **183**, 1024–1042.e21 (2020).
7. A. J. Greaney *et al*., *Cell Host Microbe* **29**, 44–57.e9 (2021).
8. A. Z. Wec *et al*., *Science* **369**, 731–736 (2020).
9. D. Pinto *et al*., *Nature* **583**, 290–295 (2020).
10. T. N. Starr *et al*., *Nature* **597**, 97–102 (2021).
11. C. A. Jette *et al*., *Cell Rep.* **36**, 109760 (2021).
12. M. A. Tortorici *et al*., *Nature* **597**, 103–108 (2021).
13. Y.-J. Park *et al*., *Science* **375**, 449–454 (2022).
14. D. R. Martinez *et al*., *Sci. Transl. Med.* **14**, eabj7125 (2022).
15. D. Pinto *et al*., *Science* **373**, 1109–1116 (2021).
16. C. Wang *et al*., *Nat. Commun.* **12**, 1715 (2021).
17. G. Song *et al*., *Nat. Commun.* **12**, 2938 (2021).
18. M. M. Sauer *et al*., *Nat. Struct. Mol. Biol.* **28**, 478–486 (2021).
19. P. Zhou *et al*., *Sci. Transl. Med.* **14**, eabi9215 (2022).
20. P. Zhou *et al*., bioRxiv 479488 [Preprint] (2022); https://doi.org/10.1101/2022.03.04.479488.
21. D. Corti *et al*., *Science* **333**, 850–856 (2011).
22. M. M. Sajadi *et al*., *Cell* **173**, 1783–1795.e14 (2018).
23. H.-X. Liao *et al*., *Nature* **496**, 469–476 (2013).
24. J. F. Scheid *et al*., *Science* **333**, 1633–1637 (2011).
25. J. Huang *et al*., *Nature* **491**, 406–412 (2012).
26. C. Dreyfus *et al*., *Science* **337**, 1343–1348 (2012).
27. D. Sok, D. R. Burton, *Nat. Immunol.* **19**, 1179–1188 (2018).
28. D. Corti, A. Lanzavecchia, *Annu. Rev. Immunol.* **31**, 705–742 (2013).
29. D. Pinna, D. Corti, D. Jarrossay, F. Sallusto, A. Lanzavecchia, *Eur. J. Immunol.* **39**, 1260–1270 (2009).
30. A. C. Walls *et al*., *Cell* **185**, 872–880.e3 (2022).
31. E. M. Anderson *et al*., *Cell* **184**, 1858–1864.e10 (2021).
32. M. Hoffmann *et al*., *Cell* **181**, 271–280.e8 (2020).
33. C.-L. Hsieh *et al*., *Science* **369**, 1501–1505 (2020).
34. E. Shrock *et al*., *Science* **370**, eabd4250 (2020).
35. K. W. Ng *et al*., *Science* **370**, 1339–1343 (2020).
36. C. M. Poh *et al*., *Nat. Commun.* **11**, 2806 (2020).
37. C. Daniel *et al*., *J. Virol.* **67**, 1185–1194 (1993).
38. H. Zhang *et al*., *J. Virol.* **78**, 6938–6945 (2004).
39. A. C. Walls *et al*., *Nature* **531**, 114–117 (2016).
40. Q. Xiong *et al*., bioRxiv 477490 [Preprint] (2022); https://doi.org/10.1101/2022.01.24.477490.
41. F. A. Lempp *et al*., *Nature* **598**, 342–347 (2021).
42. H. V. Dang *et al*., *Nat. Struct. Mol. Biol.* **26**, 980–987 (2019).
43. A. C. Walls *et al*., *Proc. Natl. Acad. Sci. U.S.A.* **114**, 11157–11162 (2017).
44. B. A. Johnson *et al*., *Nature* **591**, 293–299 (2021).
45. M. Hoffmann, H. Kleine-Weber, S. Pöhlmann, *Mol. Cell* **78**, 779–784.e5 (2020).
46. S. M.-C. Gobeil *et al*., *Mol. Cell* **82**, 2050–2068.e6 (2022).
47. W. Li *et al*., *Nature* **426**, 450–454 (2003).
48. V. S. Raj *et al*., *Nature* **495**, 251–254 (2013).
49. H. Hofmann *et al*., *Proc. Natl. Acad. Sci. U.S.A.* **102**, 7988–7993 (2005).
50. C. L. Yeager *et al*., *Nature* **357**, 420–422 (1992).
51. M. A. Tortorici *et al*., *Science* **370**, 950–957 (2020).
52. A. C. Walls *et al*., *Cell* **176**, 1026–1039.e15 (2019).
53. D. R. Burton, *Nat. Rev. Immunol.* **19**, 77–78 (2019).
54. M. Bonsignori *et al*., *Immunol. Rev.* **275**, 145–160 (2017).
55. J.-E. Park *et al*., *Proc. Natl. Acad. Sci. U.S.A.* **113**, 12262–12267 (2016).
56. J. K. Millet, G. R. Whittaker, *Proc. Natl. Acad. Sci. U.S.A.* **111**, 15214–15219 (2014).
57. P. V. Raghuvamsi *et al*., *eLife* **10**, e63646 (2021).
58. S. Yu *et al*., *Proc. Natl. Acad. Sci. U.S.A.* **119**, e2111199119 (2022).
59. E. Qing *et al*., *Cell Rep.* **39**, 110786 (2022).
60. C. Cheng *et al*., *PLOS ONE* **14**, e0215163 (2019).
61. K. Xu *et al*., *Nat. Med.* **24**, 857–867 (2018).
62. R. Kong *et al*., *Science* **352**, 828–833 (2016).
63. L. Ou *et al*., *Sci. Rep.* **10**, 3032 (2020).
64. R. Nachbagauer *et al*., *Nat. Med.* **27**, 106–114 (2021).
65. H. M. Yassine *et al*., *Nat. Med.* **21**, 1065–1070 (2015).
66. A. Impagliazzo *et al*., *Science* **349**, 1301–1306 (2015).
67. S. Belouzard, V. C. Chu, G. R. Whittaker, *Proc. Natl. Acad. Sci. U.S.A.* **106**, 5871–5876 (2009).
68. I. G. Madu, S. L. Roth, S. Belouzard, G. R. Whittaker, *J. Virol.* **83**, 7411–7421 (2009).
69. J. S. Low *et al*., *Science* **372**, 1336–1341 (2021).
70. M. N. Prichard, C. Shipman Jr., *Antiviral Res.* **14**, 181–205 (1990).

ACKNOWLEDGMENTS

We thank all study participants who donated blood and devoted time to our research; M. Biggiogero, A. Franzetti Pellanda, E. Picciocchi, T. Terrot, S. Tettamanti, T. Urbani, L. Vicari, and all personnel at the hospitals and nursing homes for providing blood samples; D. Vaqueirinho, S. Jovic, I. Giacchetto Sasselli, R. Schmidt, and X. Xi from the Sallusto laboratory for help with blood processing; M. Kopf (ETH Zurich) for providing the pLVX-puro-ACE2 transfer plasmid; H. Tani (University of Toyama) for providing the reagents necessary for preparing VSV pseudotyped viruses; M. Weisshaar (ETH Zurich) for his artistic rendition of fig. S1; and Y. Z. Tan from the Rubinstein laboratory for helpful discussion. **Funding:** The work was supported by the Henry Krenter Foundation (F.S.); the European Research Council (AdG no. 885539 ENGRAB to A.L.); the National Institute of Allergy and Infectious Diseases of the National Institutes of Health (grants DP1AI158186 and HHSN272201700059C to D.V.); a Pew Biomedical Scholars Award (D.V.); Investigators in the Pathogenesis of Infectious Disease Awards from the Burroughs Wellcome Fund (D.V.); Fast Grants (D.V.); the Natural Sciences and Engineering Research Council of Canada (M.M.); University of Washington Arnold and Mabel Beckman cryoEM center; the National Institutes of Health (grant S10OD032290 to D.V.); Beamline 5.0.1 at the Advanced Light Source at Lawrence Berkley National Laboratory; and EOC research funds. D.V. is an investigator of the Howard Hughes Medical Institute. F.S. and the Institute for Research in Biomedicine are supported by the Helmut Horten Foundation. **Competing interests:** J.S.L., J.J., F.S., A.L., and A.Ca. are currently listed as inventors on multiple patent applications, which disclose the subject matter described in this manuscript. A.L., D.C., F.S., J.N., M.M.-R., L.A.P., G.S., and D.P. hold shares in Vir Biotechnology. The Veesler laboratory and the Sallusto laboratory have received sponsored research agreements from Vir Biotechnology Inc. The remaining authors declare no competing interests. **Author contributions:** Conceptualization: J.S.L., M.A.T., A.L., D.V., F.S.; Funding acquisition: F.S., D.V., A.L.; Investigation: J.S.L., J.J., M.A.T., M.M., D.P., A.C., S.B., J.E.B., A.J., C.S., M.R., A.C.W., D.M., F.M., P.P., D.J., M.F., R.A., B.W., J.No., J.Ne., M.M., L.A.P., C.G., P.F., A.Ce.; Methodology: J.S.L., J.J., M.A.T., M.M., D.P., A.C., S.B., J.E.B., A.J., A.C.W., D.M., F.M., P.P., D.J., M.F., R.A., B.W., J.No.; Supervision: J.S.L., D.C., D.V., A.L., F.S.; Writing, review and editing: J.S.L., M.A.T., G.S., D.C., D.V., A.L., F.S. **Data and materials availability:** All data associated with this manuscript are available in the main text or the supplementary materials, including the FACS data gating strategy. The crystal structures were deposited to the Protein Data Bank with accession numbers listed in table S3. All further relevant source data that support the findings of this study are available from the corresponding authors upon reasonable request. Materials are available through materials transfer agreements (UBMTAs or similar agreements) with the Institute for Research in Biomedicine and the University of Washington.

SUPPLEMENTARY MATERIALS

science.org/doi/10.1126/science.abq2679
Materials and Methods
Figs. S1 to S8
Tables S1 to S5
References (*71–106*)
MDAR Reproducibility Checklist

Submitted 28 March 2022; accepted 3 July 2022
10.1126/science.abq2679